



ELSEVIER

Contents lists available at ScienceDirect

## Data in brief

journal homepage: [www.elsevier.com/locate/dib](http://www.elsevier.com/locate/dib)

## Data Article

# Data on time series analysis of land surface temperature variation in response to vegetation indices in twelve Wereda of Ethiopia using mono window, split window algorithm and spectral radiance model



A.S. Mohammed Abdul Athick<sup>a, b, c</sup>, K. Shankar<sup>d, \*</sup>,  
Hasan Raja Naqvi<sup>e</sup>

<sup>a</sup> Taiwan International Graduate Program (TIGP) – Earth System Science Program, Academia Sinica, Taipei 11529, Taiwan

<sup>b</sup> Graduate Institute of Hydrology and Oceanic Science, National Central University, Taoyuan, Taiwan

<sup>c</sup> Research Center for Environmental Changes, Academia Sinica, Taipei, Taiwan

<sup>d</sup> Department of Applied Geology, School of Applied Natural Science, Adama Science & Technology University, Ethiopia

<sup>e</sup> Department of Geography, Faculty of Natural Sciences, Jamia Millia Islamia (A Central University), New Delhi 110025, India

## ARTICLE INFO

*Article history:*

Received 30 June 2019

Received in revised form 18 October 2019

Accepted 31 October 2019

Available online 9 November 2019

*Keywords:*

Land surface temperature (LST)

Normalized difference vegetation index (NDVI)

Mono window

Split window algorithm

Spectral radiance model

## ABSTRACT

In the past, decadal time-series analysis has been done traditionally using meteorological data. In particular, decadal analysis of land surface temperature has been a major issue due to the unavailability of remote sensing techniques. But, nowadays, with the recent advances in remote sensing techniques and modern software Land Surface Temperature (LST) can be calculated through the thermal bands. LST can be estimated through many algorithms such as Split-window, Mono-Window (SW), Single-Channel (SH), among others. LST was estimated using Mono-Window algorithm on Landsat-5 TM, Landsat-7 ETM+ and split window algorithm on Landsat-8 OLI/TIRS Thermal Infrared (TIR) bands. Vegetation index was obtained by using Normalized Difference Vegetation Index (NDVI) from red and Near-Infrared (NIR) bands. NDVI has been effectively used in vegetation monitoring and to analyze the vegetation in responses to climate change such as surface temperature variation. The twelve Weredas (third-level administrative

\* Corresponding author.

E-mail address: [geoshankar1984@gmail.com](mailto:geoshankar1984@gmail.com) (K. Shankar).

divisions) of Ethiopia which are highly prone to drought were selected to investigate decadal land surface temperature variations and its impact on the surrounding environment, especially on vegetation cover. Ten Landsat images of three different sensors from 1999 to 2018 were used as the basic data source. The processed data of surface temperature and vegetation indices showed a strong correlation. The higher LST values indicate the smaller NDVI and vice versa and it is also identified the areas with high temperature being barren regions and areas with low temperature covered with more vegetation.

© 2019 Published by Elsevier Inc. This is an open access article under the CC BY-NC-ND license (<http://creativecommons.org/licenses/by-nc-nd/4.0/>).

Specification Table

|                            |   |
|----------------------------|---|
| Subject Area               | Land Surface Temperature and Environmental Studies  |
| More specific subject Area | Land Surface Temperature and Vegetation Indices   |
| Type of data               | Table, figure and text file   |
| How data was acquired      | Data were extracted from various Landsat sensors such as ETM+, TM and OLI TIRS with path/row numbers 168/54 and primary data of air temperature was obtained from Ethiopian meteorological agency.  |
| Data format                | Raw and Analyzed  |
| Experimental factors       | We make use of data from USGS and Ethiopian meteorological agency for mapping change in surface temperature and its impact on vegetation and vice versa.  |
| Experimental features      | The data were radiometrically corrected using spectral radiance model. The land surface temperature and vegetation indices were calculated employing Mono window, split window and NDVI algorithm, using Thermal bands NIR and Red band respectively in R Studio. |
| Data source location       | Landsat ETM+, TM and OLI TIRS, twelve Wereda (8°10'–9°25'N, 38°40'–40°00'E)   |
| Data accessibility         | Data are available in this article and supplementary file   |
| Related research article   | A.S.M. Abdul Athick, K. Shankar, Data on Land Use and Land Cover Changes in Adama Wereda, Ethiopia, on ETM+, TM and OLI- TIRS landsat sensor using PCC and CDM techniques, Data in Brief, 24 (2019) [1].  |

#### Value of the Data

- The Presented datasets speculate the LST and its spatial correlation with NDVI across twelve Weredas of Ethiopia for two decades.
- The data provides information on the variation of surface temperature on drought-prone Weredas.
- The data can aid to analyze the influence of land surface temperature variation over large and as well as a small area.
- The generated data can be utilized for statistical analysis of LST, NDVI and other variables for twelve Weredas in Ethiopia.
- The data can be useful for further research in various aspects of environmental monitoring.

## 1. Data

The data discussed in this article were used to calculate the spatiotemporal variation of LST using mono, split window algorithm and land cover types based on NDVI over two decades from 1999 to 2018 for twelve Weredas (Fig. 1, Table 1). Ten Landsat images were spatially analysed using their respective thermal infrared bands and the computed LST are illustrated in Fig. 2a–j using the temperature range. The variation of minimum and maximum surface temperature is depicted in Fig. 3. The area coverage of land covers such as water bodies, sparse vegetation and dense vegetation are shown in Fig. 4a–j using their NDVI values and range used to identify the different land cover types are depicted

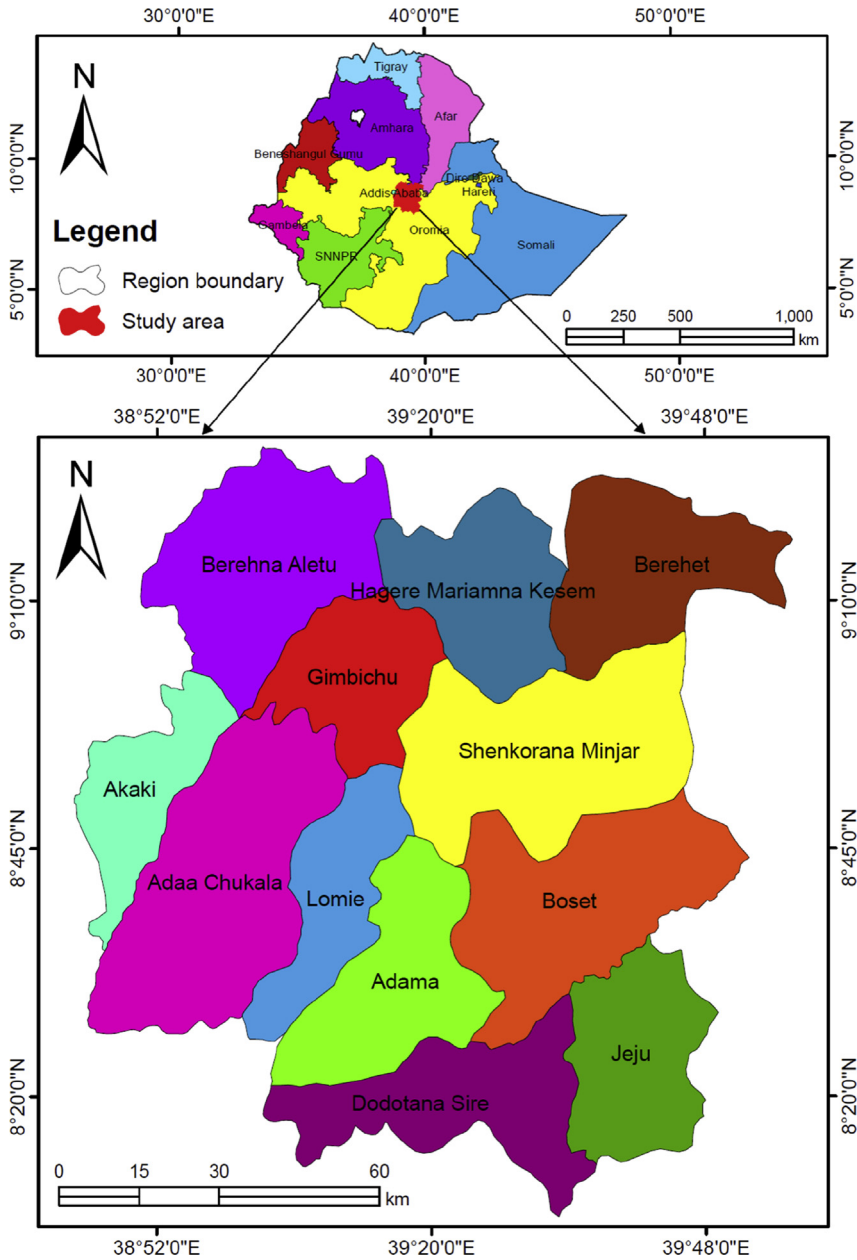


Fig. 1. Drought-prone Weredas in Ethiopia.

in Table 2 with their respective area coverage in Table 3. The minimum and maximum NDVI values for two decades are specified in Table 4. The comparison of area coverage of three land cover types and its spatial correlation with temperature are analysed in Table 5. Fig. 5 exhibits the relationship between land cover feature, temperature and respective area. The raw data provided in supplementary file.

**Table 1**  
The spatial extent of Weredas.

| S.No | Wereda                | Region | Zone        | Elevation | Area (Km <sup>2</sup> ) |
|------|-----------------------|--------|-------------|-----------|-------------------------|
| 1    | Adaa Chukala          | Oromia | East Shoa   | 1953      | 1668.9                  |
| 2    | Adama                 | Oromia | East Shoa   | 1675      | 999.3                   |
| 3    | Akaki                 | Oromia | East Shoa   | 2173      | 629.6                   |
| 4    | Berehet               | Amhara | Semien Shoa | 1442      | 996.12                  |
| 5    | Berehna Aletu         | Oromia | North Shoa  | 2707      | 1297.1                  |
| 6    | Boset                 | Oromia | East Shoa   | 1378      | 1378.5                  |
| 7    | Dodotana Sire         | Oromia | Arsi        | 1742      | 1005.4                  |
| 8    | Gimbichu              | Oromia | East Shoa   | 2305      | 737.1                   |
| 9    | Hagere Mariamna Kesem | Amhara | Semien Shoa | 2323      | 861.3                   |
| 10   | Jeju                  | Oromia | Arsi        | 1952      | 846.1                   |
| 11   | Lomie                 | Oromia | East Shoa   | 1981      | 685.9                   |
| 12   | Shenkorana Minjar     | Amhara | Semien Shoa | 1570      | 1534.7                  |

## 2. Experimental design, materials, and methods

Micro and global Climate change have been a significant issue over the last several decades. Time series cloud free remotely sensed data are acquired in different spectral bands [2] provides a powerful tool to learn from past, monitoring current scenario and also to predict the feature change. Land surface temperature and land cover have a vital role in influencing the environment and landscape attributes [3]. TM (2010, 2011), ETM+ (1999, 2000, 2003) and OLI-TIRS (2013, 2014, 2015, 2016, 2018) of overall 30 m spatial resolution and 60 m spatial resolution for TIR respective to band six in TM, ETM+ and 100 m spatial resolution for TIR1 and TIR2 respective band ten and eleven with path and row of 168/54 were the secondary data employed in this article. The primary data of air temperature was collected from automatic weather station by Ethiopian meteorological agency were utilised to validate the LST images. To begin with NIR and the red band were radiometrically corrected to remove the error due to noise from sensor and atmosphere by converting the digital number to radiance and further to reflectance using spectral radiance model.

To estimate the radiance of Landsat-5 TM (Eq. (1)) and Landsat-7 ETM+ (Eq. (2)) from digital number (DN) the following equation was used [4].

$$L_{\lambda} = L_{Min} + (L_{Max} - L_{Min}) * \frac{DN}{255} \quad (1)$$

where,  $L_{\lambda}$  is the spectral radiance,  $L_{Min}$  is the spectral radiance of DN value 1,  $L_{Max}$  is the spectral radiance of DN value at 255, and DN is the digital Number [4].

$$L_{\lambda} = \frac{(L_{Max} - L_{Min})}{(Q_{CalMax} - Q_{CalMin})} * (Q_{Cal} - Q_{CalMax}) + L_{Min} \quad (2)$$

where,  $L_{\lambda}$  is the spectral radiance at sensors aperture or the calculated radiance associated with the ground area enclosed in the pixel and referred to as the wavelength range of specific band,  $L_{Max}$  is spectral at the Sensor Radiance scaled to  $Q_{CalMax}$ ,  $L_{Min}$  is Spectral at the Sensor Radiance scaled to  $Q_{CalMin}$ ,  $Q_{CalMax}$  is the maximum quantized calibrated pixel values corresponding to  $L_{Max}$ ,  $Q_{CalMin}$  is the minimum quantized calibrated pixel value (DN) corresponding to  $L_{Min}$  and  $Q_{Cal}$  is the quantized calibration pixel value [4].

Further the obtained radiance value from Landsat -5 and 7 were converted reflectance using Eq. (3).

$$\rho P = \frac{\pi * L_{\lambda} * d^2}{E_{sun_{\lambda}} * \cos \theta_s} \quad (3)$$

where  $\rho P$  unit less planetary reflectance,  $L_{\lambda}$  represents the spectral radiance at sensors aperture,  $d$  is the earth-sun distance in astronomical units calculated from the meta data,  $E_{sun_{\lambda}}$  obtained from mean solar exo-atmospheric irradiance from table and  $\theta_s$  represents the solar zenith angle.

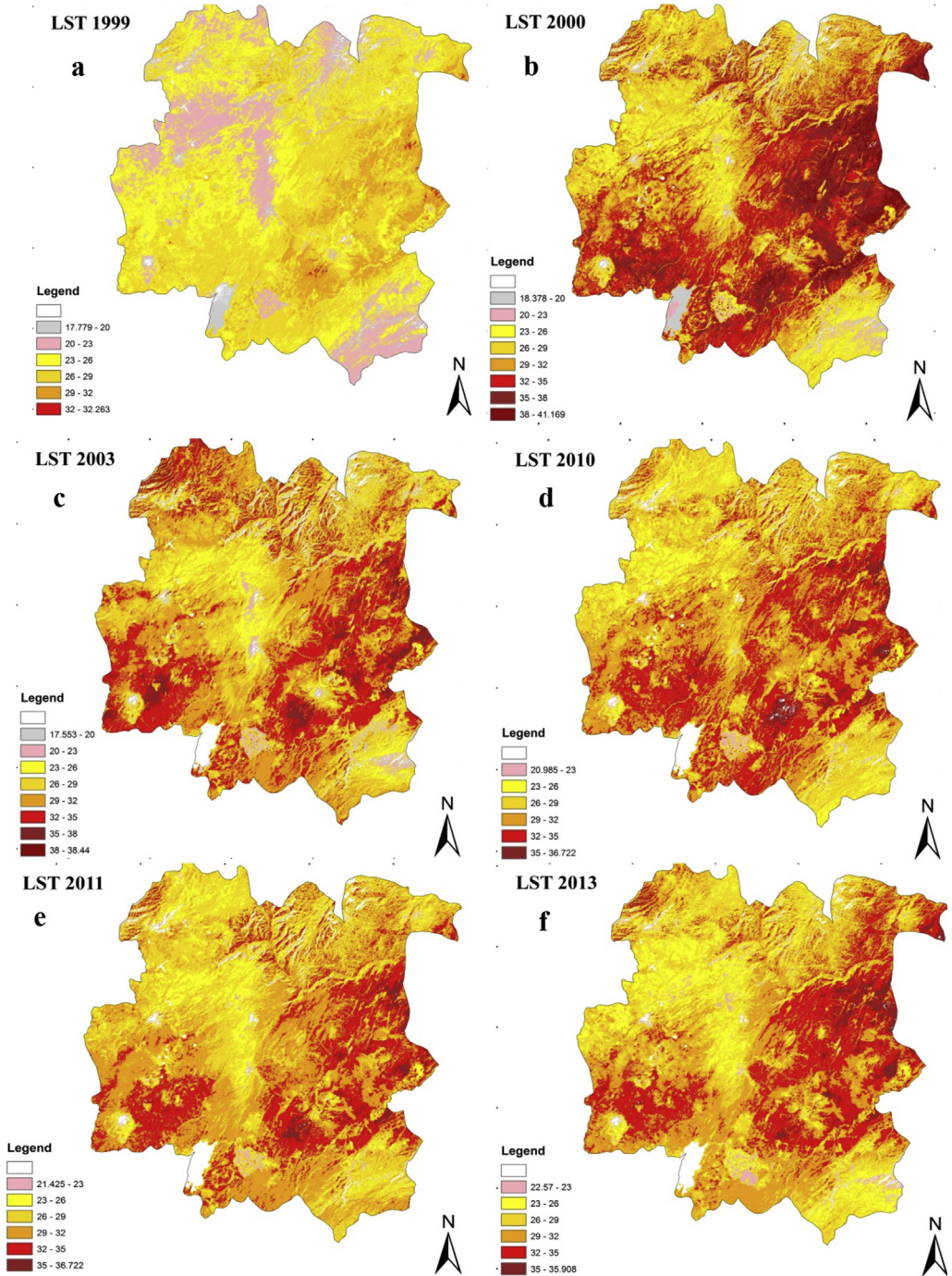


Fig. 2. LST scenario of twelve Weredas from 1999 (a) to 2018 (j).

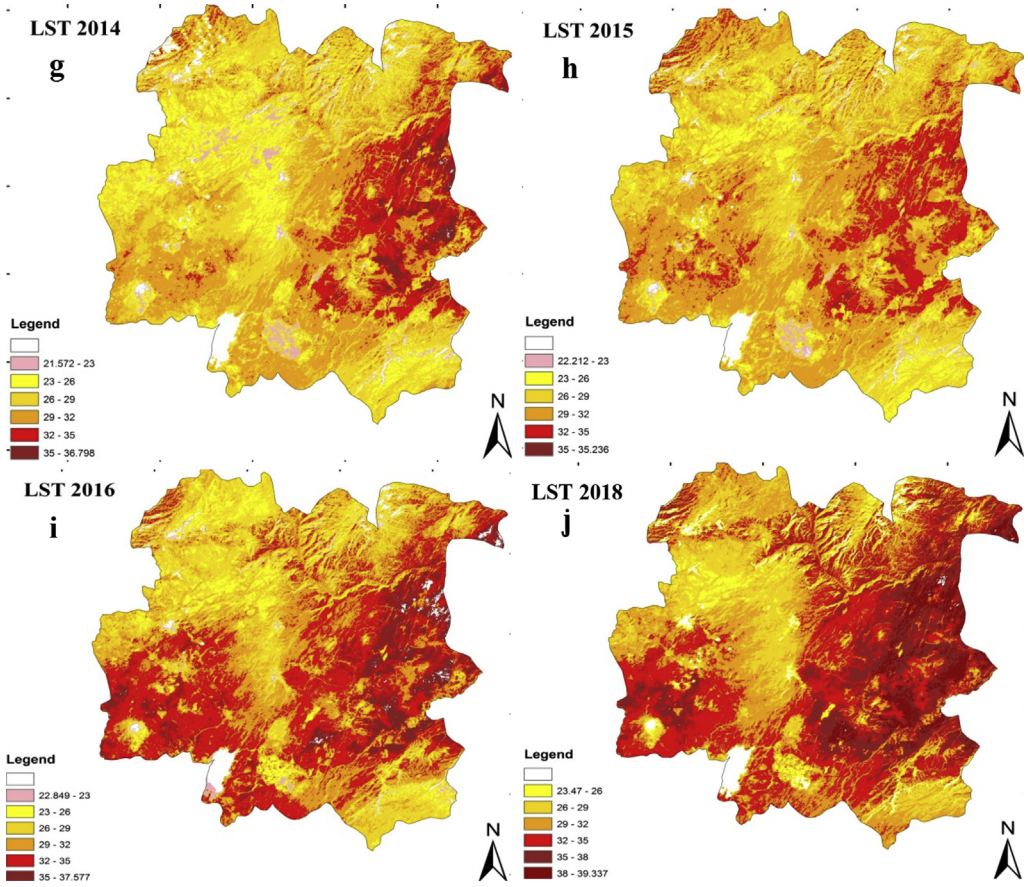


Fig. 2. (continued).

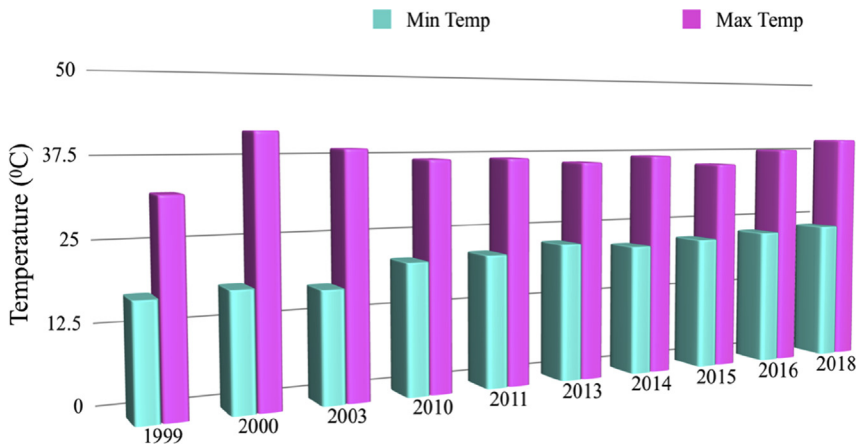


Fig. 3. Minimum and maximum surface temperature variation.

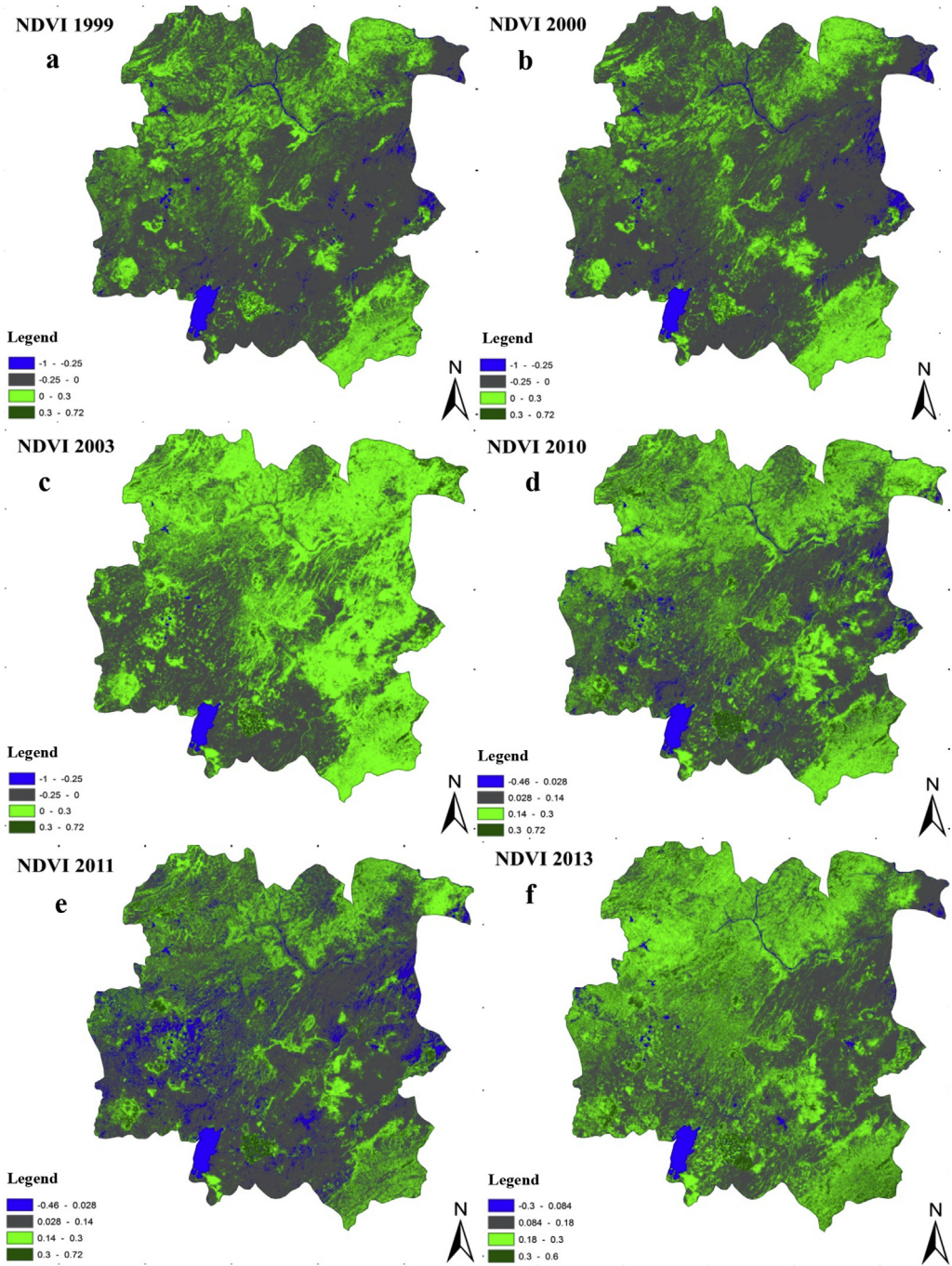


Fig. 4. Scenario of Water bodies, dense and sparse vegetation from 1999 (a) to 2018 (j).

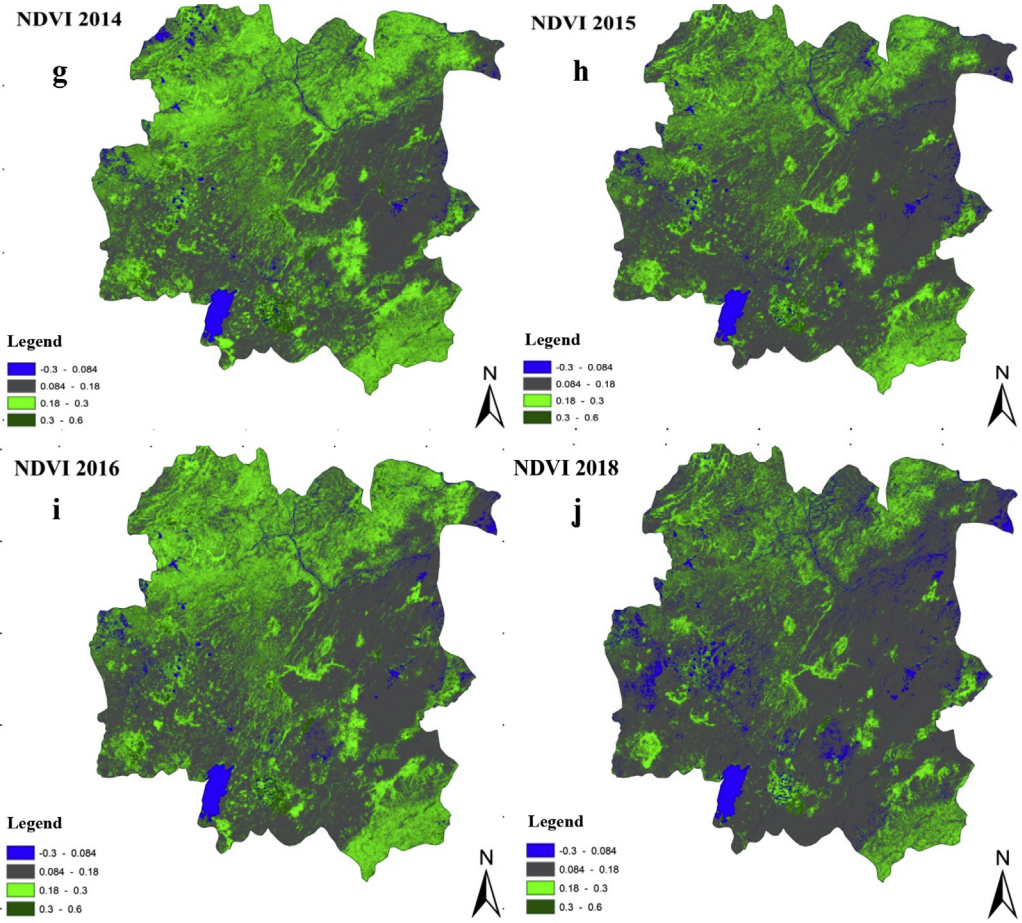
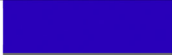


Fig. 4. (continued).

**Table 2**  
Land cover classification range based on NDVI.

| S.No | Land cover type   | Landsat-5 TM            | Landsat-7 ETM+       | Landsat-8 OLI/TIRS     | color  |
|------|-------------------|-------------------------|----------------------|------------------------|--|
| 1    | Water Bodies      | $\geq -0.46 \leq 0.028$ | $\geq -1 \leq -0.25$ | $\geq -0.3 \leq 0.084$ |  |
| 2    | Barren Area       | $>0.028 < 0.14$         | $>0.25 < 0$          | $>0.084 < 0.18$        |  |
| 3    | Sparse Vegetation | $\geq 0.14 < 0.3$       | $\geq 0 < 0.3$       | $\geq 0.18 < 0.3$      |  |
| 4    | Dense Vegetation  | $\geq 0.3 < 0.72$       | $\geq 0.3 < 0.72$    | $\geq 0.3 < 0.6$       |  |

**Table 3**

Area coverage of Land cover types.

| S.No | Year | Water bodies (hectare) | Sparse Vegetation (hectare) | Dense Vegetation (hectare) |
|------|------|------------------------|-----------------------------|----------------------------|
| 1    | 1999 | 30,827.25              | 284,304                     | 13,230.99                  |
| 2    | 2000 | 34,471.17              | 266,304.7                   | 17,204.94                  |
| 3    | 2003 | 11,017                 | 604,279.1                   | 40,497.48                  |
| 4    | 2010 | 36,625                 | 436,734.9                   | 74,115.81                  |
| 5    | 2011 | 90,989                 | 252,815.5                   | 46,334.34                  |
| 6    | 2013 | 24,748                 | 343,214.6                   | 115,047.1                  |
| 7    | 2014 | 29,823                 | 403,135.4                   | 55,068.84                  |
| 8    | 2015 | 32,927                 | 274,678.1                   | 23,976.81                  |
| 9    | 2016 | 32,810                 | 355,501.7                   | 51,117.39                  |
| 10   | 2018 | 63,275                 | 182,237.8                   | 18,660.96                  |

**Table 4**

Minimum and maximum of NDVI values for two decades.

| S·NO | NDVI image of (year) | Minimum value | Maximum value |
|------|----------------------|---------------|---------------|
| 1    | 1999                 | -0.68067      | 0.58427       |
| 2    | 2000                 | -0.99225      | 0.60656       |
| 3    | 2003                 | -0.99225      | 0.71605       |
| 4    | 2010                 | -0.44528      | 0.70213       |
| 5    | 2011                 | -0.45882      | 0.71429       |
| 6    | 2013                 | -0.25203      | 0.59245       |
| 7    | 2014                 | -0.23899      | 0.57231       |
| 8    | 2015                 | -0.22938      | 0.52663       |
| 9    | 2016                 | -0.26238      | 0.57817       |
| 10   | 2018                 | -0.24386      | 0.5475        |

Whereas the DN values are directly converted to reflectance in Landsat-8, OLI/TIRS, TIR band using the following Eq. (4).

$$p\lambda' = M_p * Q_{cal} + A_p \quad (4)$$

where  $p\lambda'$  is the Spectral reflectance,  $M_p$  is the multiplicative reflectance value,  $A_p$  is the additive reflectance value and  $Q_{cal}$  is the pixel values in DN. The obtained spectral reflectance is not true reflectance it is needed to carry out solar elevation angle correction to obtained true top of atmosphere (TOA) Eq. (5).

$$P\lambda = \frac{P\lambda'}{\sin\theta} \quad (5)$$

where  $p\lambda$  is the true planetary reflectance and  $\theta$  is the solar elevation angle.

Then the radiometrically corrected NIR and red bands were used to calculate the NDVI values from 1999 to 2018 using Eq. (6).

$$NDVI = \frac{NIR - R}{NIR + R} \quad (6)$$

Later the land cover features such as Water Bodies, Barren Area, Sparse Vegetation and Dense Vegetation [5–9] were obtained from the processed NDVI data using the ranges depicted in Table 3. Finally the LST from band six was obtained by converting the radiance value to surface temperature in Kelvin for Landsat-5 and 7 using mono window algorithm [10–12] as expressed in Eq. (7).

$$T_B = \frac{K_2}{L_n \left[ \frac{K_1}{L_i} + 1 \right]} \quad (7)$$

**Table 5**  
Comparison matrix between Land covers and LST.

| Land cover   | 1999               |       |       | 2000               |       |       | Decadal change |       |
|--------------|--------------------|-------|-------|--------------------|-------|-------|----------------|-------|
|              | Area (Ha)          | %     | Avg.T | Area (Ha)          | %     | Avg.T | Area (Ha)      | Avg.T |
| S. veg       | 2,84,304           | 86.58 |       | 2,66,044.70        | 83.74 |       | ↓              |       |
| D. veg       | 13,230.90          | 4.03  | 25.02 | 17,204.9           | 5.42  | 29.77 | ↑              | ↑     |
| WB           | 30,827.20          | 9.39  |       | 34,471.10          | 10.84 |       | ↑              |       |
| <b>Total</b> | <b>3,28,362.10</b> |       |       | <b>3,17,720.70</b> |       |       |                |       |
| Land cover   | 2000               |       |       | 2003               |       |       | Decadal change |       |
|              | Area (Ha)          | %     | Avg.T | Area (Ha)          | %     | Avg.T | Area (Ha)      | Avg.T |
| S. veg       | 2,66,044.70        | 83.74 |       | 6,04,279.10        | 92.14 |       | ↑              |       |
| D. veg       | 17,204.9           | 5.42  | 29.77 | 40,497.48          | 6.18  | 27.99 | ↑              | ↓     |
| WB           | 34,471.10          | 10.84 |       | 11,017             | 1.68  |       | ↓              |       |
| <b>Total</b> | <b>3,17,720.70</b> |       |       | <b>6,55,793.58</b> |       |       |                |       |
| Land cover   | 2003               |       |       | 2010               |       |       | Decadal change |       |
|              | Area (Ha)          | %     | Avg.T | Area (Ha)          | %     | Avg.T | Area (Ha)      | Avg.T |
| S. veg       | 6,04,279.10        | 92.14 |       | 4,36,734.90        | 79.77 |       | ↓              |       |
| D. veg       | 40,497.48          | 6.18  | 27.99 | 74,115.81          | 13.54 | 28.86 | ↑              | ↑     |
| WB           | 11,017             | 1.68  |       | 36,625             | 6.69  |       | ↑              |       |
| <b>Total</b> | <b>6,55,793.58</b> |       |       | <b>5,47,475.71</b> |       |       |                |       |
| Land cover   | 2010               |       |       | 2011               |       |       | Decadal change |       |
|              | Area (Ha)          | %     | Avg.T | Area (Ha)          | %     | Avg.T | Area (Ha)      | Avg.T |
| S. veg       | 4,36,734.90        | 79.77 |       | 2,52,815.50        | 64.8  |       | ↓              |       |
| D. veg       | 74,115.81          | 13.54 | 28.86 | 46,334.34          | 11.88 | 29.07 | ↓              | ↑     |
| WB           | 36,625             | 6.69  |       | 90,989             | 23.32 |       | ↑              |       |
| <b>Total</b> | <b>5,47,475.71</b> |       |       | <b>3,90,138.84</b> |       |       |                |       |
| Land cover   | 2011               |       |       | 2013               |       |       | Decadal change |       |
|              | Area (Ha)          | %     | Avg.T | Area (Ha)          | %     | Avg.T | Area (Ha)      | Avg.T |
| S. veg       | 2,52,815.50        | 64.8  |       | 3,43,214.60        | 71.06 |       | ↑              |       |
| D. veg       | 46,334.34          | 11.88 | 29.07 | 1,15,047.10        | 23.82 | 29.24 | ↑              | ↑     |
| WB           | 90,989             | 23.32 |       | 24,748             | 5.12  |       | ↓              |       |
| <b>Total</b> | <b>3,90,138.84</b> |       |       | <b>4,83,009.70</b> |       |       |                |       |
| Land cover   | 2013               |       |       | 2014               |       |       | Decadal change |       |
|              | Area (Ha)          | %     | Avg.T | Area (Ha)          | %     | Avg.T | Area (Ha)      | Avg.T |
| S. veg       | 3,43,214.60        | 71.06 |       | 4,03,135.40        | 82.61 |       | ↑              |       |
| D. veg       | 1,15,047.10        | 23.82 | 29.24 | 55,068.84          | 11.28 | 29.19 | ↓              | ↓     |
| WB           | 24,748             | 5.12  |       | 29,823             | 6.11  |       | ↑              |       |
| <b>Total</b> | <b>4,83,009.70</b> |       |       | <b>4,88,027.24</b> |       |       |                |       |
| Land cover   | 2014               |       |       | 2015               |       |       | Decadal change |       |
|              | Area (Ha)          | %     | Avg.T | Area (Ha)          | %     | Avg.T | Area (Ha)      | Avg.T |
| S. veg       | 4,03,135.40        | 82.61 |       | 2,74,678.10        | 82.84 |       | ↓              |       |
| D. veg       | 55,068.84          | 11.28 | 29.19 | 23,976.81          | 7.23  | 28.72 | ↓              | ↓     |
| WB           | 29,823             | 6.11  |       | 32,927             | 9.93  |       | ↑              |       |
| <b>Total</b> | <b>4,88,027.24</b> |       |       | <b>3,31,581.91</b> |       |       |                |       |
| Land cover   | 2015               |       |       | 2016               |       |       | Decadal change |       |
|              | Area (Ha)          | %     | Avg.T | Area (Ha)          | %     | Avg.T | Area (Ha)      | Avg.T |
| S. veg       | 2,74,678.10        | 82.84 |       | 3,55,501.70        | 80.9  |       | ↓              |       |
| D. veg       | 23,976.81          | 7.23  | 28.72 | 51,117.39          | 11.63 | 30.21 | ↑              | ↑     |
| WB           | 32,927             | 9.93  |       | 32,810             | 7.47  |       | ↓              |       |
| <b>Total</b> | <b>3,31,581.91</b> |       |       | <b>4,39,429.09</b> |       |       |                |       |
| Land cover   | 2016               |       |       | 2018               |       |       | Decadal change |       |
|              | Area (Ha)          | %     | Avg.T | Area (Ha)          | %     | Avg.T | Area (Ha)      | Avg.T |
| S. veg       | 3,55,501.70        | 80.9  |       | 1,82,237.80        | 68.98 |       | ↓              |       |
| D. veg       | 51,117.39          | 11.63 | 30.21 | 18,660.96          | 7.06  | 31.41 | ↓              | ↑     |
| WB           | 32,810             | 7.47  |       | 63,275             | 23.96 |       | ↑              |       |
| <b>Total</b> | <b>4,39,429.09</b> |       |       | <b>2,64,173.96</b> |       |       |                |       |

Note: S.Veg – sparse vegetation; D.Veg – Dense vegetation; WB – Water bodies; Avg.T- Average temperature; Ha-hectare; ↓ - decrease; ↑ - increase.

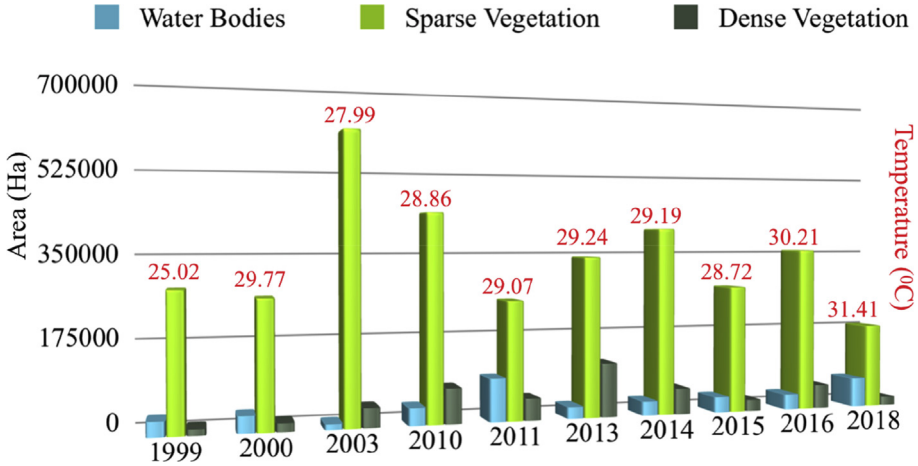


Fig. 5. Comparisons of land cover feature, area and temperature.

where, TB is the effective satellite brightness temperature in Kelvin, K1 is the calibration constant 1, K2 is the calibration constants 2, Ln is the natural logarithm, Lλ is the spectral radiance in watts [4].

The radiance value for band ten and eleven of Landsat-8 from the raw DN pixels was calculated using Eq. (8).

$$L_{\lambda} = M_L * Q_{Cal} + A_L \tag{8}$$

where L λ is the Spectral Radiance, ML is the multiplicative radiance value, AL is the additive radiance value and Qcal is the pixel values in DN.

The surface temperature using band ten and eleven from Landstat-8 was derived using the split window algorithm [13,14].

$$LST = TB_{10} + C_1(TB_{10} - TB_{11}) + C_2(TB_{10} - TB_{11})^2 + C_0 + (C_3 + C_4W)(1 - \epsilon) + (C_5 + C_6W)\Delta\epsilon \tag{9}$$

where LST = Land surface temperature, C0–C6 = Split window coefficient values, TB10 and TB11 = Brightness temperature of band 10 and band 11, ε = M band 10 and band 11, ε = Mean LSE of TIR bands, W = Atmospheric water vapor content, Δε = Difference in LSE based on the methods provided by Ref. [15] in Eq. (10).

$$TOAr = M_L * DN * A_L \tag{10}$$

where A L = Radiance add, M L = Radiance multiplier, DN = Digital number.

The Brightness temperature (TB) for both TIR bands was calculated by adapting the following Eq. (11).

$$T_B = \frac{K_2}{L_n \left[ \frac{K_1}{TOAr} + 1 \right]} \tag{11}$$

where K1 and K2 = Thermal constant for TIR bands, TB = Brightness temperature, TOAr = Atmospheric spectral radiance.

The data processed to obtain NDVI can be interpreted based on their class range Table 3. Feature such as water bodies, dense vegetation, sparse vegetation is found commonly in the input data. Before classifying the NDVI values it must be sure that values must fall between the range -1 and 1 [4]. Negative values of NDVI approaching -1 corresponds to water bodies, values close to (-0.1 to 0.1) generally indicates barren land, rock, sand or snow. Whereas positive values between 0.2 and 0.4 represent shrub and grassland. While, a high value approaching 1 indicates dense, temperate or

tropical rainforest. It may also require additionally performing the manual adjustment in the NDVI range due to the difference in sun angle and acquisition date and year. The spatially analyzed Landsat images using their thermal infrared bands clearly exhibits the surface temperature variation in 20 years from 1999 to 2018. It is identified that the minimum and maximum temperature value was least in 1999 with an average temperature of 25.02 °C and surged to the highest of 31.41 °C in 2018. Interestingly it is found that NDVI and LST show a trend of strong correlation. In many Weredas the higher NDVI implies lower LST value and vice versa. The area of land cover types also decreased in case of increasing LST. One of the drought-prone Wereda such as Adama showed a steady rise in land surface temperature with a decrease in the area of water bodies and vegetation. Hence this condition can be reversed by increasing the plantation as a part of microclimate change.

## Acknowledgments

Authors are highly thankful to the Adama and Addis Ababa Meteorology agencies are appreciated for providing metrological data. Our hearty thanks to the Editor-in-Chief and anonymous reviewer for his valuable suggestions to improve in the present form.

## Conflict of Interest

The authors declare that they have no known competing financial interests or personal relationships that could have appeared to influence the work reported in this paper.

## Appendix A. Supplementary data

Supplementary data to this article can be found online at <https://doi.org/10.1016/j.dib.2019.104773>.

## References

- [1] A.S.M. Abdul Athick, K. Shankar, Data on land use and land cover changes in Adama Wereda, Ethiopia, on ETM+, TM and OLI-TIRS landsat sensor using PCC and CDM techniques, Data in Brief (2019) 24, <https://doi.org/10.1016/j.dib.2019.103880>.
- [2] A.S.M.A. Athick, H.R. Naqvi, A method for compositing MODIS images to remove cloud cover over Himalayas for snow cover mapping, in: IEEE International Geoscience and Remote Sensing Symposium (IGARSS), Beijing, 2016, pp. 4901–4904, <https://doi.org/10.1109/IGARSS.2016.7730279>.
- [3] Tamam Emiru, Hasan Raja Naqvi, Mohammed Abdul Athick, Anthropogenic impact on land use land cover: influence on weather and vegetation in Bambasi Wereda, Ethiopia, Spat. Inf. Res. 26 (4) (2018) 427–436, <https://doi.org/10.1007/s41324-018-0186-y>.
- [4] B. Tafesse, K.V. Suryabagavan, Systematic modeling of impacts of land-use and land-cover changes on land surface temperature in Adama Zuria District, Ethiopia, Model. Earth Syst. Environ. 5 (2019) 805, <https://doi.org/10.1007/s40808-018-0567-1>.
- [5] A.S. Mohammed, A. A. H.R. Naqvi, Z. Firdouse, An assessment and identification of avalanche hazard sites in Uri sector and its surroundings on Himalayan mountain, J. Mt. Sci. 12 (6) (2015), <https://doi.org/10.1007/s11629-014-3274-z>.
- [6] M. Mohan, S.K. Pathan, K. Narendrareddy, A. Kandya, S. Pandey, Dynamics of urbanization and its impact on land use land cover: a case study of Mega city Delhi, J. Environ. Prot. 2 (2011) 1274–1283, <https://doi.org/10.4236/jep.2011.29147>.
- [7] M. Thompson, Standard land cover classification scheme for remote sensing application in South Africa, South Afr. J. Sci. 92 (1996) 34–42.
- [8] R. Manandhar, I.O.A. Odeh, T. Ancev, Improving the accuracy of land use and land cover classification of landsat data using post-classification enhancement, Remote Sens. 1 (2009) 330–344, <https://doi.org/10.3390/rs1030330>.
- [9] N.S. Kawo, K. Shankar, Groundwater quality assessment using water quality index and GIS technique in Modjo River Basin, central Ethiopia, J. Afr. Earth Sci. 147 (2018) 300–311, <https://doi.org/10.1016/j.jafrearsci.2018.06.034>.
- [10] L.M. McMillin, Estimation of sea surface temperatures from two infrared window measurements with different absorption, J. Geophys. Res. 80 (1975) 5113–5117, <https://doi.org/10.1029/JC080i036p05113>.
- [11] L.M. McMillin, D.S. Crosby, Theory and validation of the multiple window sea surface temperature technique, J. Geophys. Res. 89 (1984) 3655–3661, <https://doi.org/10.1029/JC089iC03p03655>.
- [12] L. Vlassova, F. Perez-Cabello, H. Nieto, P. Martín, D. Riaño de la J. Riva, Assessment of methods for land surface temperature retrieval from Landsat-5 TM images applicable to multiscale tree-grass ecosystem modeling, Remote Sens. 6 (2014) 4345–4368, <https://doi.org/10.3390/rs6054345>.
- [13] R. Kumar, S. Singh, Case study for change detection analysis and land surface temperature retrieval in Uttarakhand Region and their correlation, Imperial J Interdiscip Res 2 (2016) 1821–1825.
- [14] N. Kayet, K. Pathak, A. Chakrabarty, S. Sahoo, Spatial impact of land use/land cover change on surface temperature distribution in Saranda Forest, Jharkhand, Model Earth Syst Environ 2 (2016) 127, <https://doi.org/10.1007/s40808-016-0159-x>.
- [15] G. Chandler, B.L. Markham, Revised Landsat-5 TM radiometric calibration procedures, and postcalibration dynamic ranges, IEEE Trans. Geosci. Remote Sens. 41 (2003) 2674–2677, <https://doi.org/10.1109/TGRS.2003.818464>.